

Submitted to *Metallurgical Transactions*, June 2000

EFFECTS OF PT INCORPORATION ON THE ISOTHERMAL OXIDATION BEHAVIOR OF CVD ALUMINIDE COATINGS

Y. Zhang^{1*}, J.A. Haynes²⁺, W.Y. Lee³, I.G. Wright², B.A. Pint², K.M. Cooley², and P.K. Liaw¹

¹The University of Tennessee, Knoxville, TN

²Oak Ridge National Laboratory, Oak Ridge, TN

³Stevens Institute of Technology, Hoboken, NJ

*Y. Zhang is currently with Walbar Metals, Peabody, MA.

⁺Direct all correspondence to J.A. Haynes, P.O. Box 2008, Oak Ridge, TN 37831-6063

Keywords: bond coating, TBC, oxidation, platinum, aluminides, sulfur

ABSTRACT

The effects of Pt incorporation on the isothermal oxidation and diffusion behavior of low-sulfur aluminide bond coatings were investigated. Aluminide (NiAl) coatings and Pt-modified aluminide (Ni,Pt)Al coatings were synthesized on a low-sulfur, yttrium-free single-crystal Ni-based superalloy by a high-purity, low-activity chemical vapor deposition (CVD) aluminizing procedure. The isothermal oxidation kinetics and scale adhesion behavior of CVD NiAl and (Ni,Pt)Al were compared at 1150°C. Compositional profiles of alloying elements in the NiAl and (Ni,Pt)Al coatings before and after isothermal oxidation were determined by electron microprobe analysis. Platinum did not reduce oxide scale growth kinetics. No significant differences in bulk refractory metal (W, Ta, Re, and Mo) distributions were observed as a result of Pt incorporation. Spallation of the alumina scale and the formation of large voids along the oxide-metal interface were commonly observed over the NiAl coating grain

boundaries after 100h at 1150°C. In contrast, no spallation of Al₂O₃ scales occurred on (Ni,Pt)Al coating surfaces or grain boundaries, although the sulfur content in the CVD (Ni,Pt)Al coatings was higher than that of the CVD NiAl coatings. Most significantly, no voids were observed at the oxide-metal interface on (Ni,Pt)Al coating surfaces or cross-sections after 200h at 1150°C. It was concluded that a major beneficial effect of Pt incorporation on aluminide coating oxidation resistance is the elimination of void growth at the oxide-metal interface, likely by mitigation of detrimental sulfur effects.

1. INTRODUCTION

Currently, state-of-the-art thermal barrier coating (TBC) systems are comprised of two layers; (1) a strain-tolerant ceramic top coat, Y₂O₃-stabilized-ZrO₂ (YSZ), and (2) a metallic bond coat, which typically consists of a plasma-sprayed NiCoCrAlY or a diffusion aluminide. The ceramic top coat provides thermal insulation, while the metallic bond coat provides oxidation protection to the superalloy substrate by forming a protective Al₂O₃ scale along the YSZ-bond coat interface. This Al₂O₃ scale is typically considered to be chemically bonded to the overlying ceramic top coat when the YSZ is fabricated by electron beam-physical vapor deposition (EB-PVD). Failure of EB-PVD TBCs typically initiates by fracture and delamination of the brittle Al₂O₃ scale along the scale-bond coat interface, which results in spallation of the ceramic top coat [1-4] and concomitant loss of thermal protection. From this perspective, development of bond coats with significantly improved Al₂O₃ scale adherence is a critical step in improving the performance of state-of-the-art TBC systems.

A common method of improving the oxidation resistance of aluminide coatings is to incorporate Pt [5, 6], although the mechanism by which Pt exerts its beneficial effects is not well-understood. Most previous work in this area has focused on platinum aluminide coatings fabricated by pack cementation, which results in a surface layer of either PtAl₂ or [PtAl₂ + (Ni,Pt)Al] [7-9]. More recently, a low-activity platinum aluminide coating, which exhibits a

surface layer of single-phase (Ni,Pt)Al instead of PtAl₂ or [PtAl₂ + (Ni,Pt)Al], has been developed via low Al activity CVD processing [10, 11]. This single-phase (Ni,Pt)Al coating has been incorporated as a bond coat for commercial EB-PVD TBC systems. There has been limited evaluation of low activity platinum aluminide bond coatings, although the available results indicate improvements in cyclic oxidation behavior, hot corrosion resistance, thermal stability, and ductility, as compared to platinum aluminide coatings fabricated by pack cementation [11-13].

In general, it appears that the positive influence of Pt primarily involves an improvement in Al₂O₃ scale adherence. A variety of mechanisms to explain the beneficial effects of Pt have been proposed, including (1) reductions in oxide growth stresses [14], (2) enhanced diffusion of Al in the coating [15], (3) mechanical keying by alloy protrusions into the scale [16], (4) inhibition of refractory-metal diffusion from the substrate into the coating and scale [17], and (5) suppression of void formation along the scale/metal interface [18, 19]. However, all of the above mechanisms have been proposed based on analysis of conventional PtAl₂ or [PtAl₂ + (Ni,Pt)Al] coatings or cast versions of (Ni,Pt)Al. Considerable interest currently exists in the examination of the effects of Pt on the oxidation behavior of single-phase CVD (Ni,Pt)Al bond coatings.

Alloy desulfurization is a recent approach to improving scale adherence in single-crystal superalloys. The beneficial effects of sulfur removal on the oxidation resistance of Ni-based alloys have been relatively well documented [20 - 23]. Our previous work [24] took this concept one step further and demonstrated that reducing the sulfur content of a low-activity CVD NiAl coating on a desulfurized, Y-free superalloy provided significant improvements in Al₂O₃ scale adherence during cyclic oxidation at 1150°C. However, localized Al₂O₃ spallation eventually occurred over the NiAl coating grain boundaries. More recent results [25, 26] indicated that Pt incorporation into these single phase CVD aluminide coatings exhibited a remarkable ability to retard scale spallation over coating grain boundaries during cyclic oxidation

testing at 1150°C, even though the sulfur levels in the CVD (Ni,Pt)Al were significantly higher than those of the low-sulfur CVD NiAl (due to contamination of the Pt during the electroplating process). A major objective of the present work was to investigate and compare the isothermal oxidation behavior (i.e., coating composition, scale growth kinetics, void formation and scale adherence) of NiAl and (Ni,Pt)Al coatings, in order to further advance our understanding of the beneficial effects of Pt on the oxidation resistance of aluminide coatings.

2. EXPERIMENTAL

An yttrium-free single-crystal Ni-based superalloy, René N5[']* (PCC Airfoils, Cleveland, OH) was used as the substrate material in this study. The nominal alloy composition (in weight percent) was determined by inductively coupled plasma analysis as: 6.05% Al, 0.05% C, 7.33% Co, 7.03% Cr, 0.15% Hf, 1.4% Mo, 3.05% Re, 6.42% Ta, 0.01% Ti, 5.13% W, and Ni as the remainder. The bulk sulfur content of this melt-desulfurized alloy was ~0.4 ppmw, as measured by glow-discharge mass spectroscopy (GDMS) 34/24Lee]. Flat specimen coupons (1.8 cm x 1.4 cm x 0.15 cm) of René N5' were polished through 0.05 μm alumina on all surfaces, followed by ultrasonic cleaning in acetone and methanol prior to coating.

Low-sulfur NiAl coatings were fabricated on René N5' by a conventional CVD aluminizing procedure (modified so as to minimize process-related sulfur contamination) at 1100°C for 6 hours, as described previously [24]. The (Ni,Pt)Al coatings were synthesized by first electroplating the substrates with ~7 μm of platinum (deposited by Howmet Corporation, Whitehall, MI) and then aluminizing the electroplated substrate by the identical CVD procedures (and CVD reactor) that were used to fabricate the low-sulfur NiAl coatings [24, 25]. As discussed previously, both processes result in an outward-growing layer of single-phase β-NiAl or β-(Ni,Pt)Al, with an underlying interdiffusion zone consisting of refractory metal-rich precipitates in a β matrix [25].

* René N5' is used here to denote a yttrium-free version of René N5.

The sulfur level in the β -phase surface layer of the as-deposited NiAl coating was measured at less than 0.5 ppmw by glow-discharge mass spectroscopy (GDMS) [24]. An increase in sulfur content to ~ 2.5 ppmw was measured at the NiAl coating/substrate interface region by GDMS sputter depth-profiling. The sulfur level in most of the β -phase layer of the as-deposited (Ni,Pt)Al coating was similar to that in the NiAl coating (less than 0.5 ppmw), but there was a sulfur peak of ~ 3 ppmw at the gas surface of the (Ni,Pt)Al coating [25]. More significantly, the sulfur content in the (Ni,Pt)Al coating increased to ~ 140 ppmw in the region where the sputtered depth coincided with the approximate location of the original Pt layer. It was previously demonstrated that this significant increase in sulfur near the original substrate interface was due to contamination of the Pt during the electroplating process [25].

Selected coated specimens, uncoated superalloy substrates (low-S, Y-free) and a cast

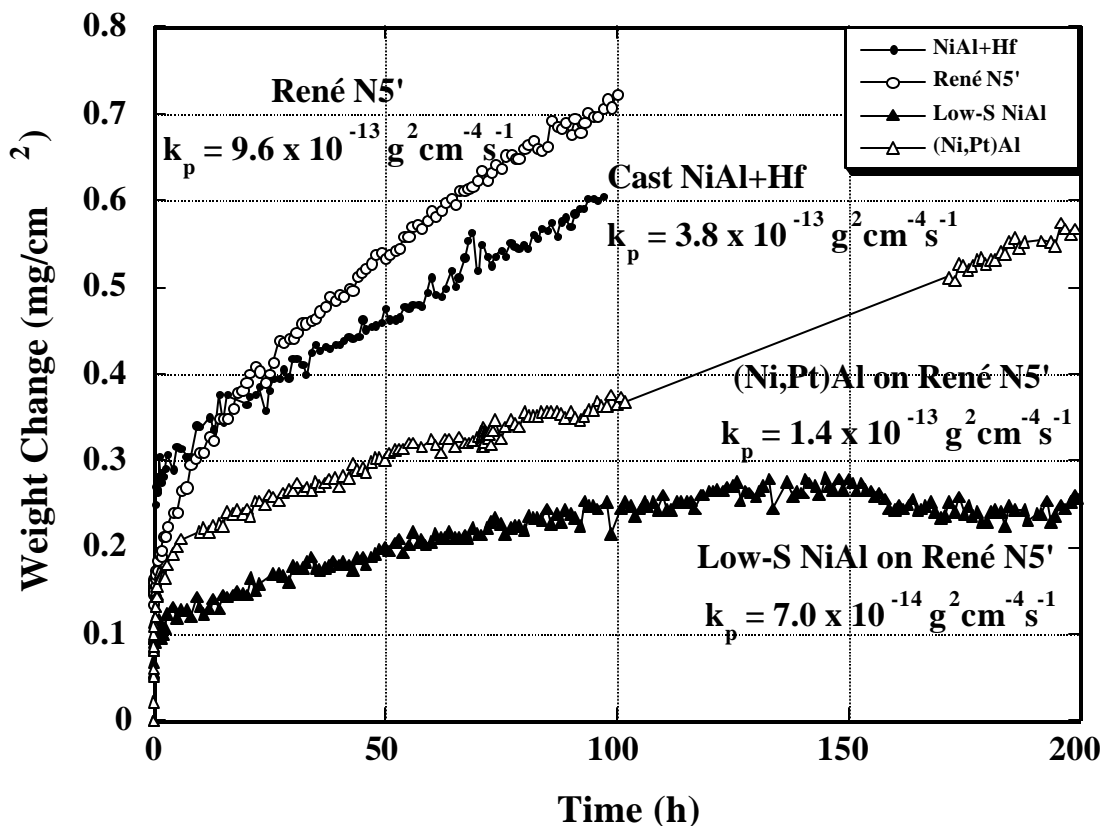


Fig. 1. Comparison of isothermal oxidation kinetics of the (Ni,Pt)Al coating with the low-sulfur NiAl coating, uncoated René N5', and a cast NiAl+Hf.

3. RESULTS

3.1. Isothermal Oxidation Kinetics of CVD NiAl and CVD (Ni,Pt)Al Coatings

The isothermal oxidation mass changes (at 1150°C) for the (Ni,Pt)Al-coated specimens are compared with NiAl-coated specimens, as well as uncoated René N5' substrates and cast NiAl + Hf (0.05at% Hf, from Ref. 27), in Fig. 1. Parabolic oxidation rate constants, k_p , were calculated from the steady-state portions of the mass gain curves and are compared for specimens oxidized for 100 or 200-h in Table I. Steady state oxide growth rates on both coatings were lower than that of cast NiAl doped with Hf (Fig. 1). Scale growth kinetics on the (Ni,Pt)Al coatings were slightly higher than those on the NiAl coatings at 1150°C (Fig. 1) and the steady-state scale growth rates on both coatings were much lower than those of the uncoated René N5'. X-ray diffraction detected α -Al₂O₃ on all oxidized coatings.

Table I. The k_p values and oxide scale thickness for CVD NiAl and (Ni,Pt)Al coatings after isothermal exposure during thermogravimetric analysis.

| Coating | Oxidation Time (h) | k_p ($g^2cm^{-4}s^{-1}$) | Measured Scale Thickness (μm) | Calculated Scale Thickness (μm) ^b |
|-----------|--------------------|---------------------------------|--------------------------------------|---|
| NiAl | 100 | ----- ^a | 1.2 \pm 0.40 | 0.9 |
| | 200 | 0.7×10^{-13} | 1.9 \pm 0.50 | 1.2 |
| (Ni,Pt)Al | 100 | 3.0×10^{-13} | 1.6 \pm 0.64 | 1.8 |
| | 200 | 1.4×10^{-13} | 2.3 \pm 0.93 | 1.7 |

^a – kinetics data lost due to computer failure, however, total specific mass gain at 100 h matched that of the 200 h specimen at 100 h.

^b Scale thickness calculated based on the total mass gain

There was significant non-uniformity in oxide scale thickness when viewed in cross-section. The average thickness of the Al_2O_3 scales after 100- and 200-h, as measured from a series of cross-sectional micrographs, ranged from 1.2 to 2.3 μm (Table I). These values were slightly greater than the thickness values calculated from the mass gains as shown in Table I. Although the oxide thickness appeared to be lower on NiAl, when data scatter was accounted for the measured average values were similar on both coatings. Scales on (Ni,Pt)Al after 200-h were especially non-uniform in thickness, in some locations varying in thickness from 0.5 to 4.0 μm over a 15 μm length of surface (with no evidence of scale loss due to cracking or spallation). Networks of small Al_2O_3 ridges were visible on the scale surfaces [Fig. 2(a) and (b)] of both coatings, as is commonly observed after oxidation of aluminides [28]. However, there were noticeable differences in the cross-sectional morphologies of the scales. Scales on (Ni,Pt)Al also contained small periodic metallic protrusions that extended from the metal into the oxide layer [arrows in Fig. 2(b)], as has been previously reported on cast PtAl alloys [16]. This effect was less pronounced after 200-h, as compared to 100-h. The oxide-metal interfaces on the NiAl coatings were much more regular in shape [Fig. 2(a)].

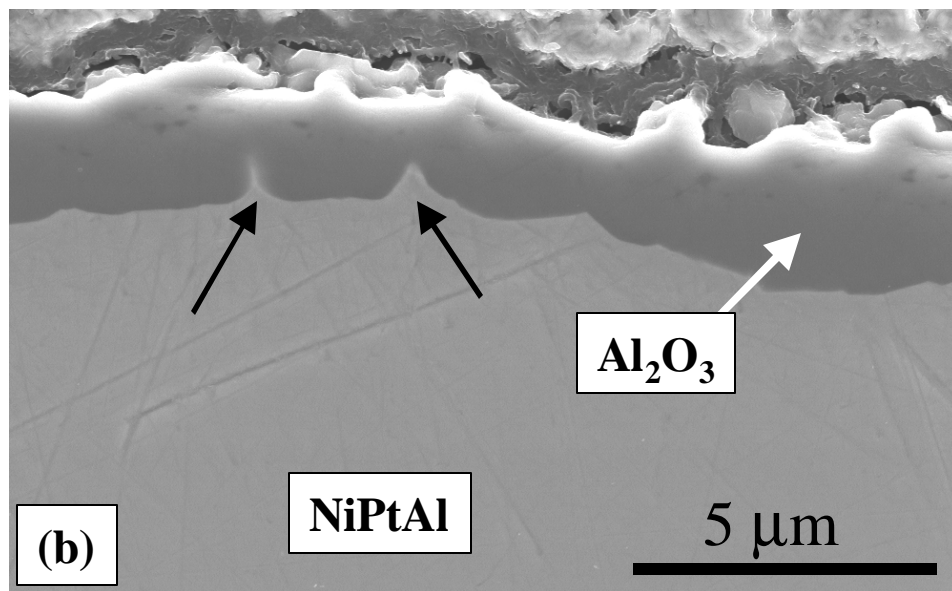
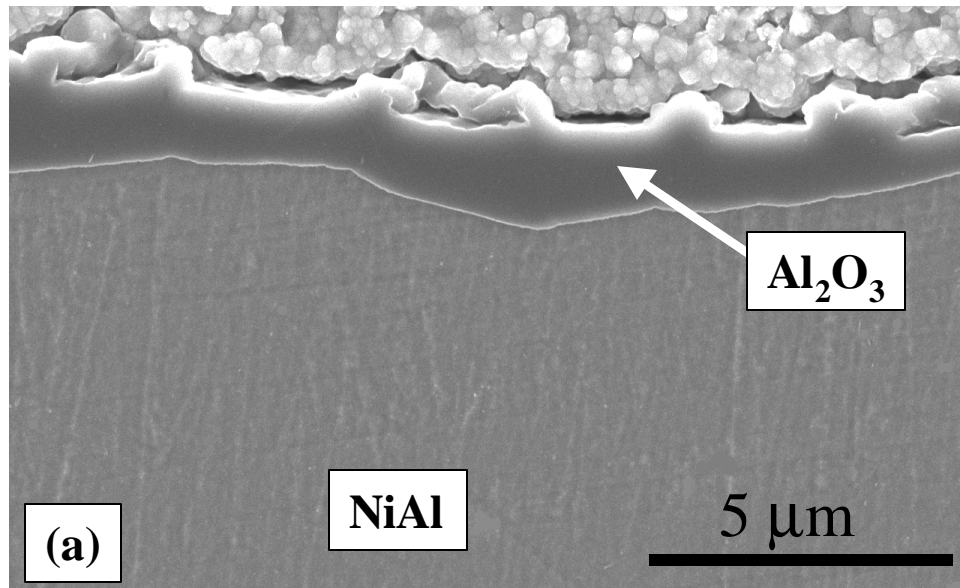


Fig. 2. SEM images of alumina scale cross-sections on aluminide coatings after 200-h oxidation at 1150°C. (a) CVD NiAl. (b) CVD (Ni,Pt)Al. The material at the top of the images is Cu plating.

3.2. Microstructural Changes of NiAl and (Ni,Pt)Al Coatings after Isothermal Oxidation at 1150°C

The surface morphologies of the as-deposited NiAl and (Ni,Pt)Al coatings have been previously described in detail [25]. Both coatings consisted of large, polygonal aluminide grains (40-120 μm in diameter) with flat surfaces. These grains were outlined with a distinct network of prominent grain boundary surface ridges (1 – 4 μm in height). In cross-section, it was apparent that the individual grains were columnar in nature, with each grain boundary extending from the original superalloy surface to the coating surface. The as-deposited NiAl and (Ni,Pt)Al coatings exhibited single-phase β -NiAl type crystal structures (by XRD). Both types of coating were typically highly textured, with the majority of the columnar coating grains rotated around the [111] direction [25].

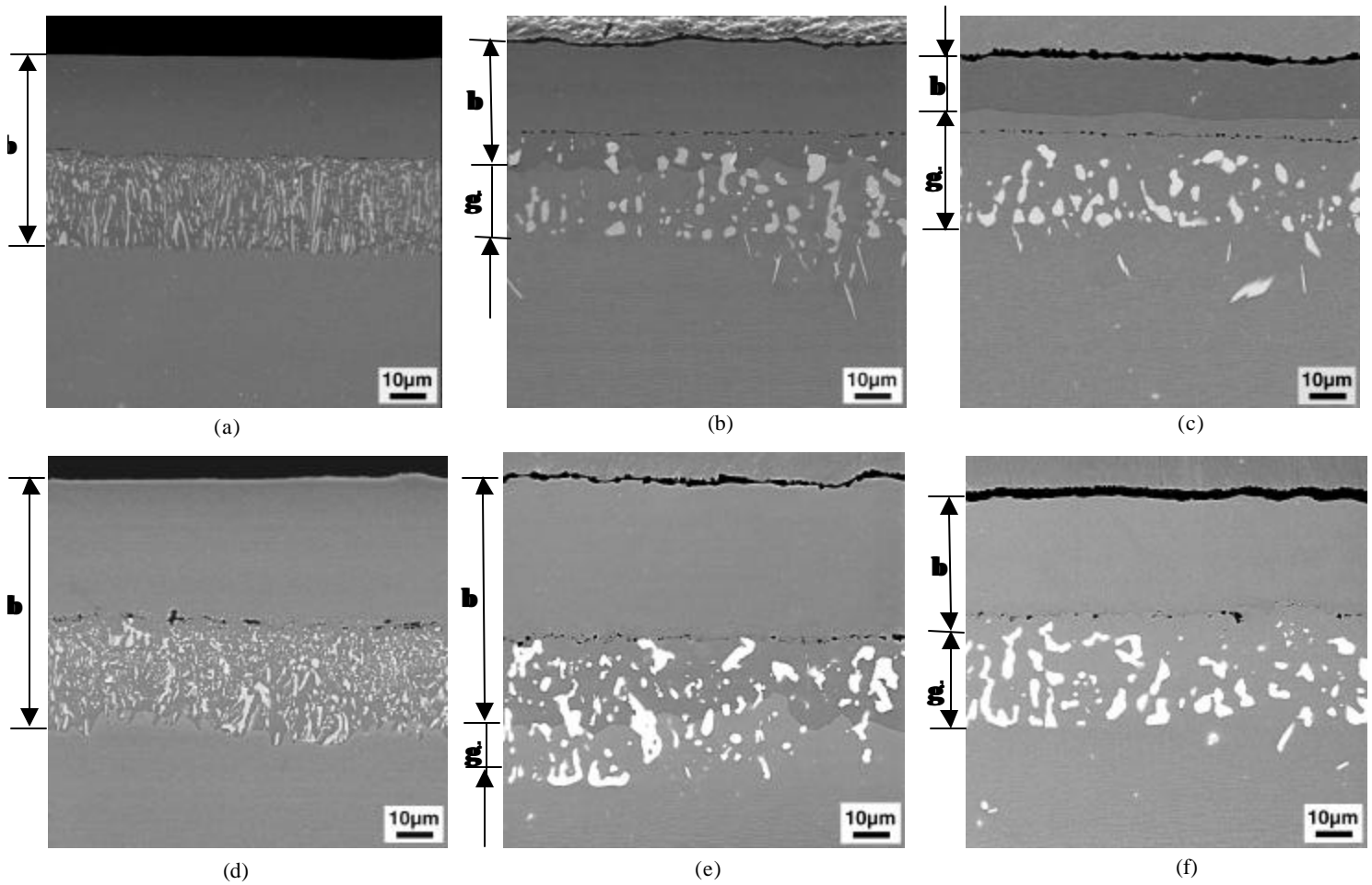


Fig. 3. SEM secondary electron images showing coating microstructural changes before and after isothermal oxidation at 1150°C: (a) as-deposited low-sulfur NiAl coating; (b) NiAl after 100h oxidation; (c) NiAl after 200h oxidation; (d) as-deposited single-phase (Ni,Pt)Al coating; (e) (Ni,Pt)Al after 100h oxidation; (f) (Ni,Pt)Al after 200h oxidation.

Figures 3(a)-(f) compare metallographic cross sections of as-deposited NiAl and (Ni,Pt)Al coatings, and show the microstructural changes which occurred during 100- or 200-h isothermal oxidation at 1150°C. The darker contrast phase in the surface layer of Figs. 3(a) – (f) is the Al-rich β -phase (the β -phase is more difficult to resolve in NiPtAl due to the Pt effect on phase contrast). The extent of internal penetration of the β phase is denoted by the arrows on each image. The original superalloy surface in all coatings contained a non-continuous planar array of small alumina particles. In the as-deposited coatings the interdiffusion zone (which began at the original superalloy surface and extended into the superalloy) consisted of brighter-contrast, elongated precipitates (rich in refractory elements) in a β -matrix, as shown in Figs.

3(a) and (d). These elongated refractory-rich (W, Ta, Re, Mo, and Cr) precipitates in the coating diffusion zone coarsened considerably during oxidation.

The overall combined thickness of the β phase (in the coating layer and interdiffusion zone) decreased with increasing exposure time at 1150°C, due to Al loss (and Ni enrichment) by interdiffusion between the coating and substrate, as well as by surface oxidation. These reductions in Al concentration resulted in localized transformation of the β phase into γ' (Ni_3Al) on the substrate side of the β -layer. Although significant decreases in total β phase thickness occurred for all specimens, a continuous surface layer of the β phase was maintained in contact with the alumina scale after 200-h exposure for all NiAl and (Ni,Pt)Al coating specimens. There was no apparent growth in the diameter of the aluminide coating grains in either system after exposure at 1150°C.

The estimated original β -phase thickness (including the β matrix of the interdiffusion zone), the measured thickness of the remaining β phase after oxidation, and the estimated amount of β -phase consumed during oxidation/interdiffusion are presented in Table II. Thickness of the as-deposited β -phase (which included the interdiffusion zone) for each NiAl specimen was estimated as 2X that of the distance from the coating surface to the alumina particles at the coating-substrate interface, since in the as-deposited NiAl coatings the diffusion zone thickness was approximately equal to the single-phase coating thickness. The thickness of the β -phase in the interdiffusion zone of as-deposited (Ni,Pt)Al was measurably less than that of the single-phase surface region (approximately 80%), and the shape of the diffusion zone-substrate interface was much more irregular than that observed beneath the NiAl coatings. Thus, the original thickness of (Ni,Pt)Al coatings was estimated at 1.8X that of the single-phase layer thickness. The thickness estimations in Table II also assume no significant movement of the small alumina particles that were initially present on the superalloy surface. There were variations in the original coating thickness of each type of coating, with the (Ni,Pt)Al coatings

generally exhibiting a greater thickness (which was at least partially due to the added thickness of the electroplated Pt layer). However, it was estimated that similar absolute amounts of β -phase were depleted in both types of coatings after 100- and 200-h isothermal oxidation when variations in measured remaining β thickness were considered.

Table II. Depletion of the β phase in NiAl and (Ni,Pt)Al coatings

| Type of Coating | Estimated Original β Thickness (mm) ^a | Oxidation Time (h) | Measured Remaining β Thickness (mm) ^b | Estimated β Thickness Reduction (mm) |
|-----------------|--|--------------------|--|--|
| NiAl | 51 | 100 | 33.6 \pm 3.6 | 17.4 |
| NiAl | 39 | 200 | 12.5 \pm 4.4 | 26.5 |
| (Ni,Pt)Al | 77 | 100 | 65.6 \pm 13 | 11.4 |
| (Ni,Pt)Al | 52 | 200 | 29.9 \pm 6.0 | 22.1 |

^a – Estimates include β matrix in diffusion zone. Sections were not cut from each specimen prior to oxidation so the exact original coating thickness was not measured. Based on ratios measured from as-deposited specimens, the original thickness of β in the oxidized NiAl specimens was estimated as 2X the thickness of the single-phase layer. A factor of 1.8X was used for estimating original β thickness in (Ni,Pt)Al.

^b – Measured from metallographic cross-sections.

3.3. Compositional Changes of NiAl and (Ni,Pt)Al Coatings after Oxidation

Compositional line profiles across NiAl and (Ni,Pt)Al coating cross-sections were obtained by EPMA at 20 kV, with a spot size of \sim 1.0 μ m and a measurement interval of \sim 2

μm . No post deposition heat treatment was employed in the present study, so it should be emphasized that the β -phase coatings [Fig. 4(a)] were not necessarily compositionally homogenized in the as-deposited condition. Figures 4(a)-(f) show the profiles for the major elements in the as-deposited condition and after 100-h and 200-h oxidation at 1150°C. Figures 5(a)-(f) show compositional profiles for the refractory elements after the same time periods.

In the as-coated condition, the concentration of Al was relatively uniform throughout the single-phase region of the NiAl coating, with an average concentration of ~39.8 at% (~23 wt%). The average atomic concentration of Al in the as-deposited (Ni,Pt)Al single-phase region was 39.6 at% (~20 wt%), very similar to the as-deposited NiAl. However, the Al concentration profile of the (Ni,Pt)Al was less uniform than in NiAl, and Al appeared to increase toward the coating surface of (Ni,Pt)Al, with a noticeable decrease in the Pt content and increase in Ni content near the surface.

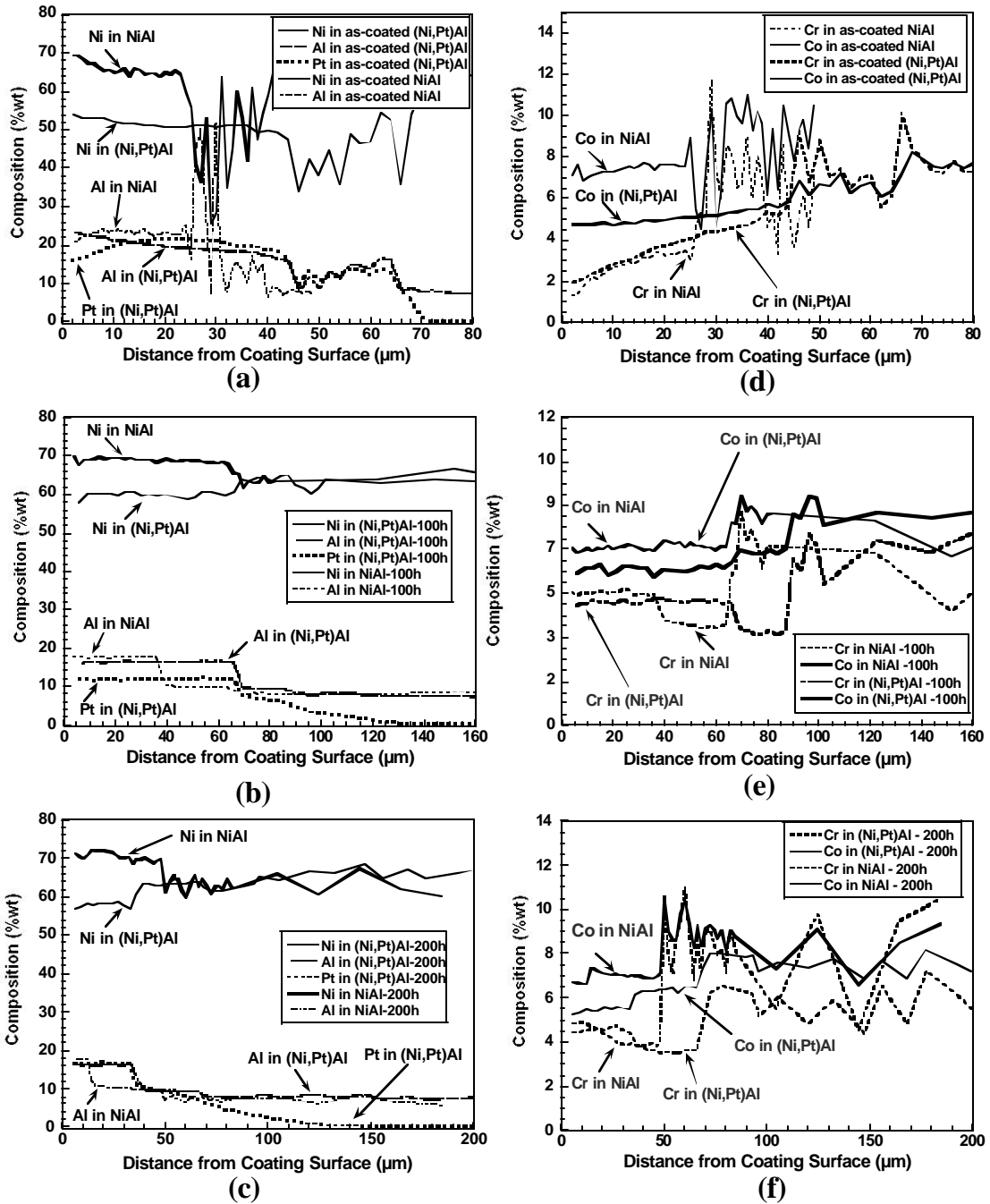


Fig. 4. Compositional profiles of major elements measured by EPMA through the thickness of NiAl and (Ni,Pt)Al coatings before and after isothermal oxidation at 1150°C: (a) Ni, Al, and Pt in as-deposited coatings; (b) Ni, Al, and Pt in coatings after 100h oxidation; (c) Ni, Al, and Pt in coatings after 200h oxidation; (d) Co and Cr in as-deposited coatings; (e) Co and Cr in coatings after 100h oxidation; (f) Co and Cr in coatings after 200h oxidation.

The Ni, Al and Pt compositional profiles were more uniform in both coatings after homogenization during the 1150°C oxidation exposures for 100 or 200 h [Figs. 4(b) and 4(c)]. The average Al concentration in the β -phase of both NiAl and (Ni,Pt)Al was reduced to ~32 at% (~17 wt%) after a 100-h exposure at 1150°C, as a result of both oxidation and interdiffusion with the substrate alloy. The Al concentration in the β -phase of both coatings remained essentially the same (~32 at%) after 200-h, although the thickness of the β -phase decreased. Localized transformation of β to γ' at the substrate interface is obvious from the abrupt decrease in the Al compositional profiles in Figs. 4(b) and (c), as well as the phase contrast of Figs. 2(b), (c), (e), and (f).

The average concentrations of alloying elements in the β and γ' phases of the NiAl and (Ni,Pt)Al coatings (as measured by EPMA) are summarized in Tables III and IV. There was significant incorporation of Co and Cr [Figs. 4(d) ~ 4(f)] from the substrate into the as-deposited β -phase of both coatings, but their concentrations did not change significantly during isothermal oxidation. The levels of refractory metal elements (W, Ta, Re and Mo) were similar and very low (less than 1 wt%, which is below the effective resolution of the electron microprobe technique) in the β -phase of both coatings in the as-deposited condition. The refractory concentration did not significantly change after 100 and 200-h isothermal oxidation [Figs. 5(a)-(f)]. However, the concentrations of the refractory metals were significantly higher (up to 7.8 wt%) in the γ' regions that formed by Al-depletion, (Table IV) due to higher solubility in the Ni₃Al phase. Also, as shown in Figs. 5(a) – (f) the local concentrations of refractory elements varied drastically in the interdiffusion zone due to the presence of precipitates rich in refractory elements (Fig. 3). In summary, there were no obvious differences in the refractory metal concentrations in the β -phase region of the bulk coatings due to Pt incorporation.

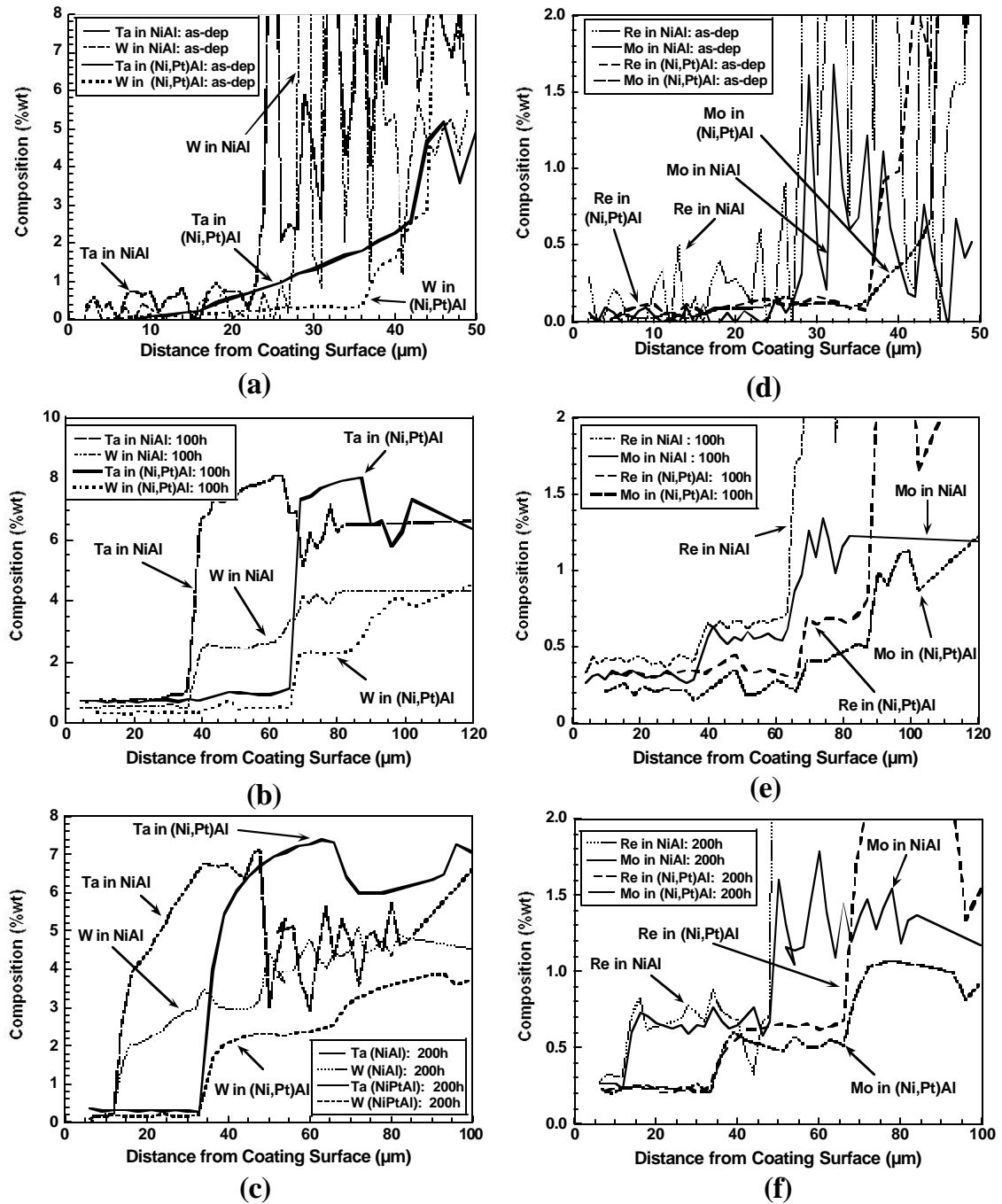


Fig. 5. Compositional profiles of refractory elements measured by EPMA through the thickness of NiAl and (Ni,Pt)Al coatings: (a) Ta and W in as-deposited coatings; (b) Ta and W in coatings after 100h oxidation; (c) Ta and W in coatings after 200h oxidation; (d) Re and Mo in as-deposited coatings; (e) Re and Mo in coatings after 100h oxidation; (f) Re and Mo in coatings after 200h oxidation.

Of additional interest was the observation that the columnar grain boundaries of the oxidized NiAl and (Ni,Pt)Al coatings were decorated with very fine, brighter-contrast particles, as shown in the cross-sectional SEM backscattered electron images of Fig. 6.

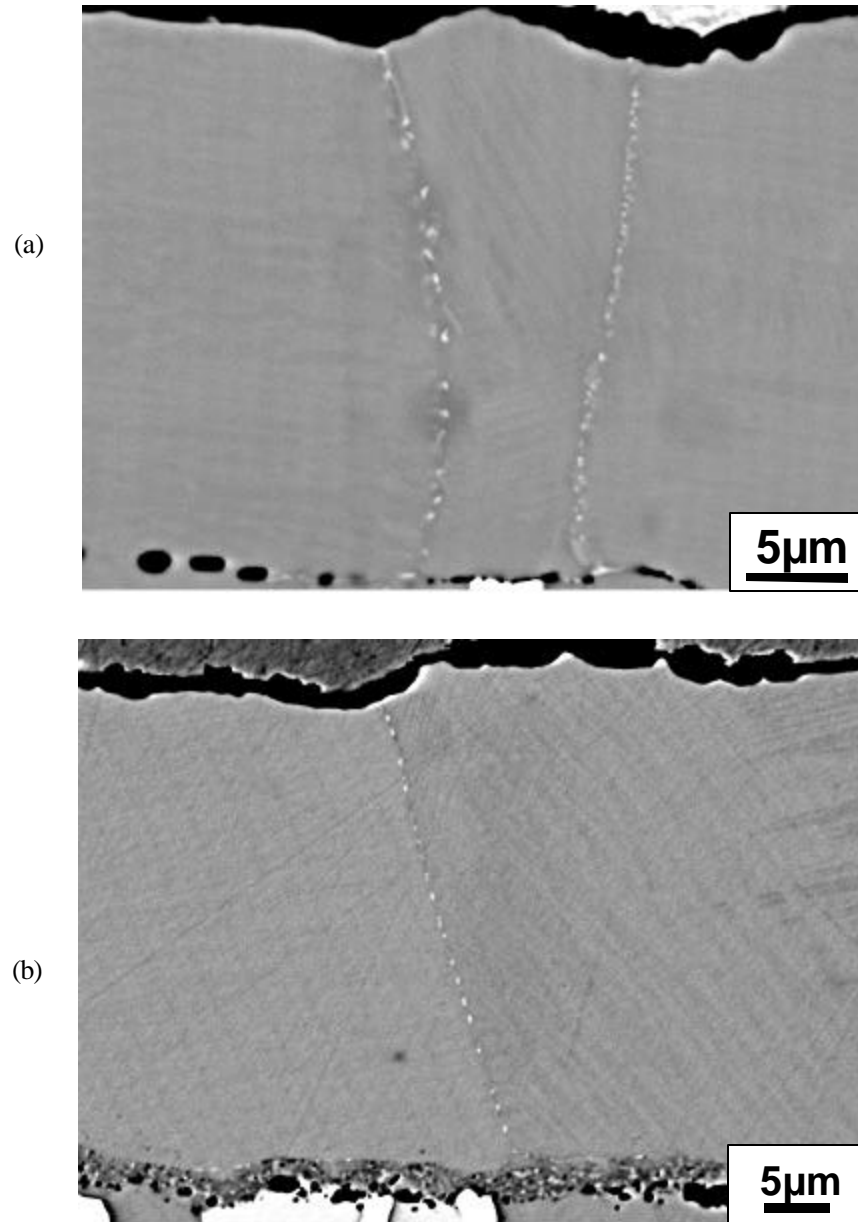


Fig. 6. SEM backscattered electron image of metallographic cross sections of the NiAl and (Ni,Pt)Al coatings after isothermal oxidation at 1150°C, indicating that fine particles segregated to coating grain boundaries: (a) NiAl after 100h oxidation; (b) (Ni,Pt)Al after 100h oxidation.

Similar particles were observed at the coating grain boundaries of as-deposited NiAl and (Ni,Pt)Al coatings after etching [24]. The diameter of these grain-boundary particles ranged from 100-400 nm. A FEG-SEM equipped with EDS and WDS verified that these particles were rich in refractory metal elements, as compared to the bulk coating grains. The EDS

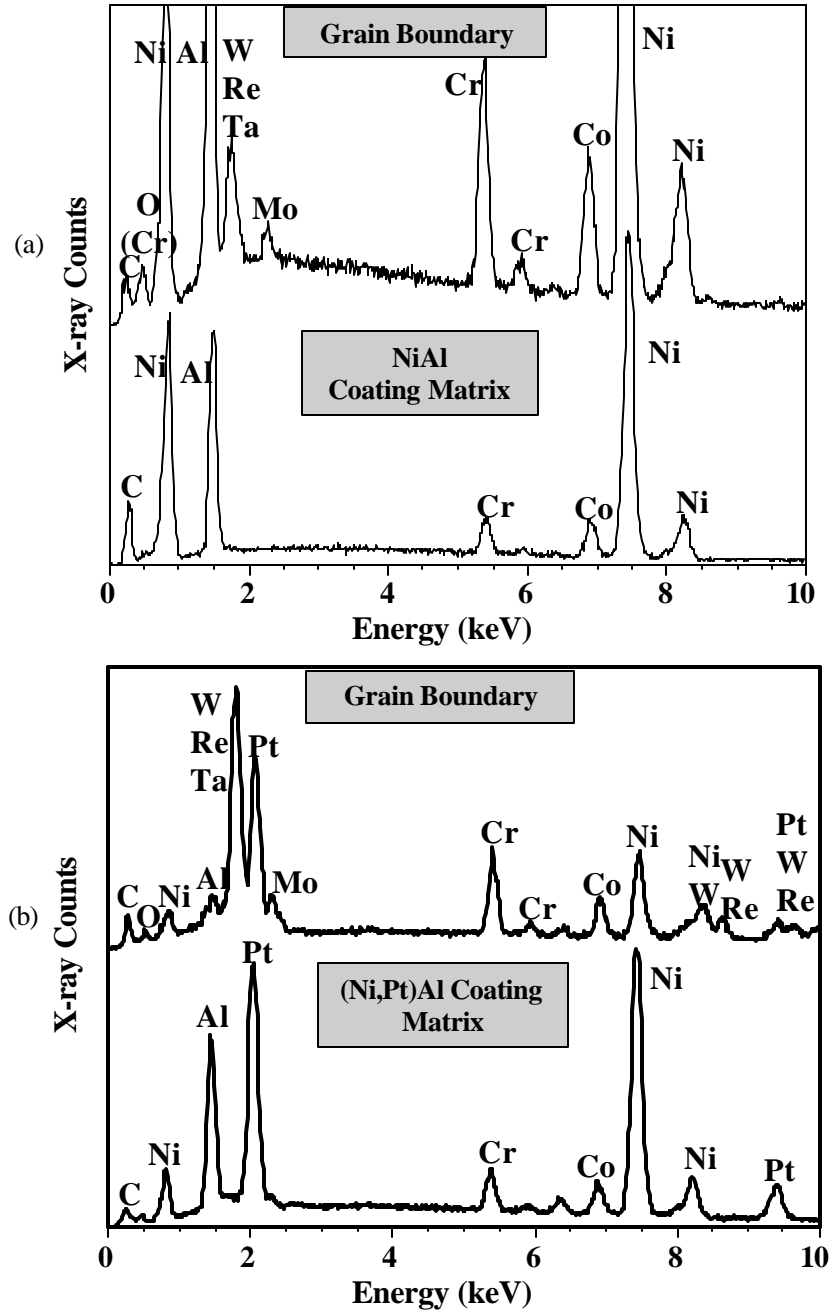


Fig. 7. FEG-SEM EDS spectra for the NiAl and (Ni,Pt)Al coatings and the particles segregated to coating grain boundaries shown in Fig. 6.

spectra of the grain boundary particles are compared to those of the bulk coatings in Fig. 7. The additional peaks on the spectra of the grain boundary particles were from W, Re, Mo, and Ta. However, the particles were too small to obtain an exact composition. There were no observable differences in grain boundary particle size or amount as a result of Pt additions.

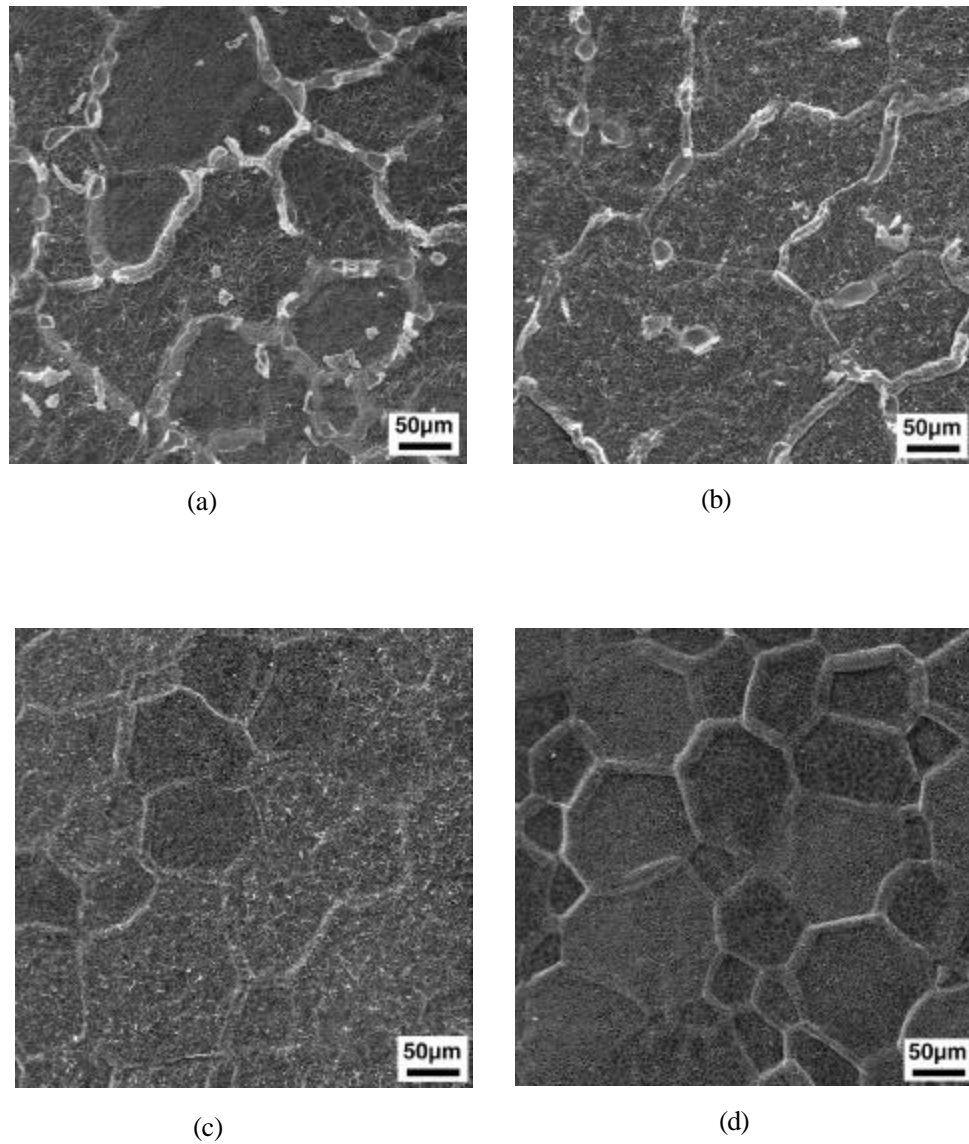


Fig. 8. SEM secondary electron image of surface morphologies of the NiAl and (Ni,Pt)Al-coated specimens after 100h and 200h oxidation at 1150°C: (a) NiAl after 100h; (b) NiAl after 200h; (c) (Ni,Pt)Al after 100h; (d) (Ni,Pt)Al after 200h.

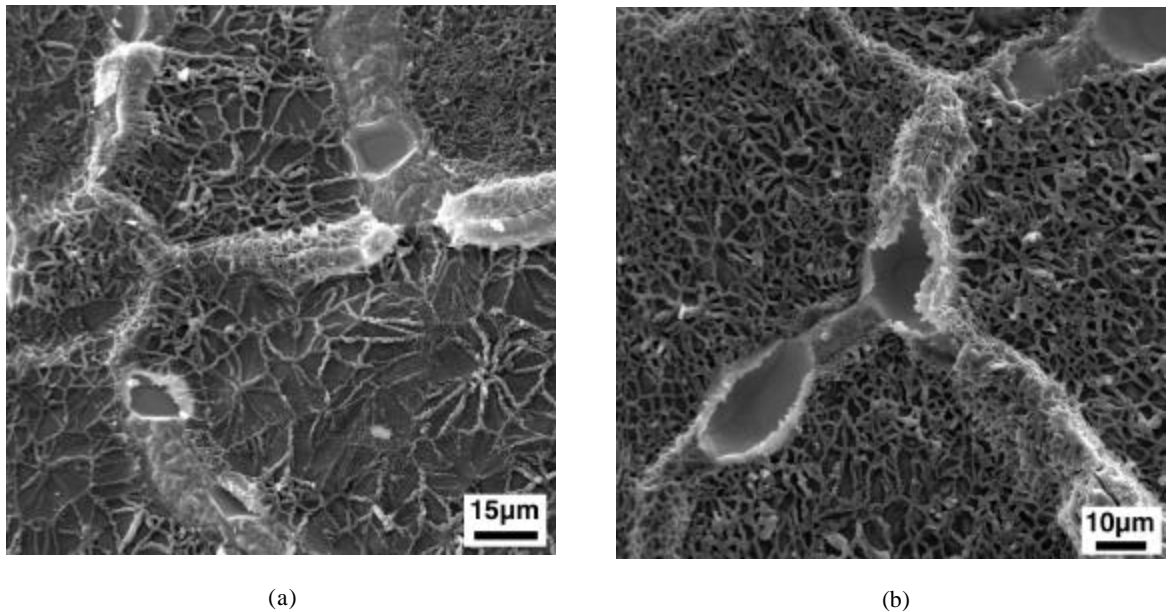


Fig. 9. SEM secondary electron images showing voids formed along NiAl coating grain boundaries after isothermal oxidation at 1150°C; (a) after 100h oxidation; (b) after 200h oxidation.

3.4. Oxide Morphologies and Scale Adherence on NiAl and (Ni,Pt)Al Coatings

The incorporation of Pt did not exert an obvious influence on the surface morphology of the protective Al_2O_3 scales that formed during isothermal oxidation. The plan view surface morphologies of the oxide scales on NiAl and (Ni,Pt)Al coating specimens after 100- and 200-h oxidation at 1150°C are shown in the SEM images of Figs. 8 and 9. The Al_2O_3 scales on both coatings showed the commonly observed oxide ridges (which are also visible in cross-section in Fig. 2) or the so-called "lacy structure" [28]. However, there were abrupt variations between alumina grains in the density of the observed Al_2O_3 ridges (which are not to be confused with the aluminide coating grain boundary ridges) on both types of coatings, as has previously been attributed to the effect of differing substrate grain orientations on the epitaxial formation of the transient cubic alumina phases [29].

There was substantial evidence of reduced scale adherence, as well as drastic differences in void growth at the oxide-metal interface, on aluminide coatings without Pt additions. The scales on the bulk NiAl grains were adherent after a 100-h isothermal exposure,

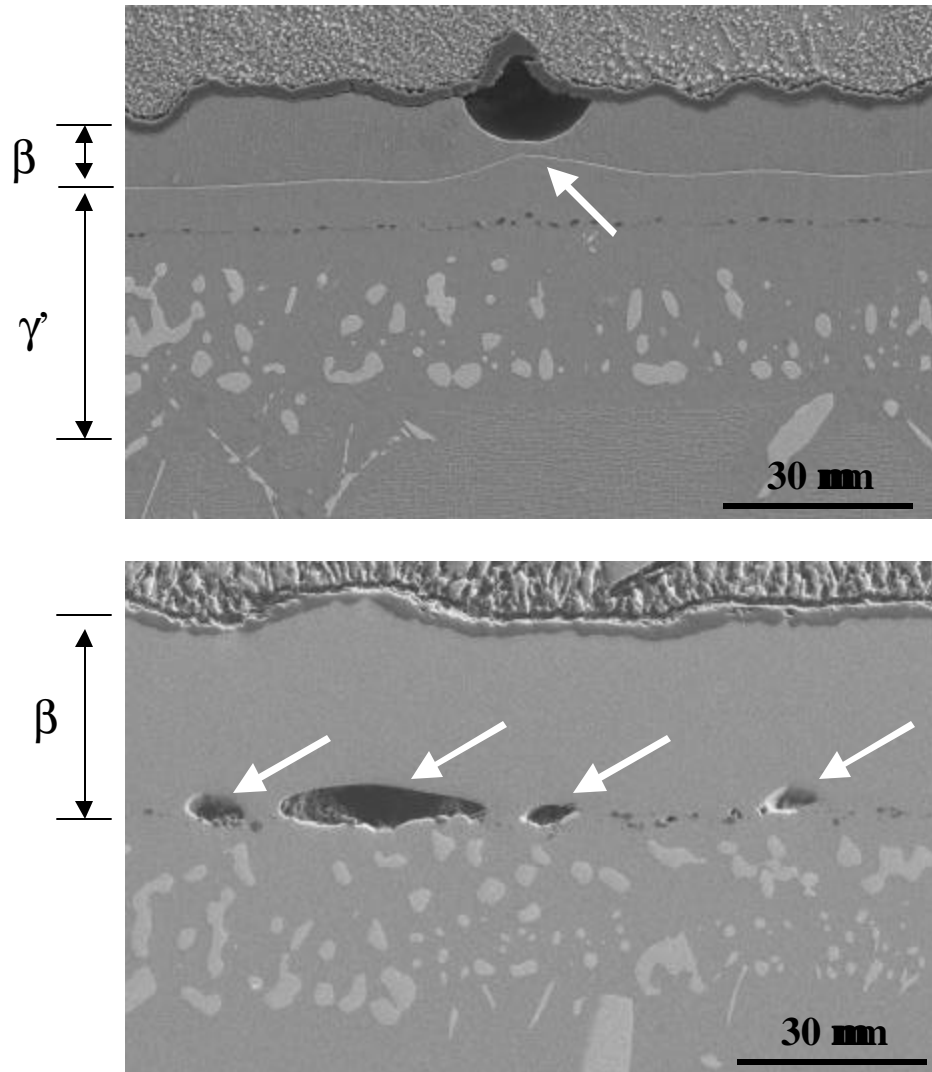


Fig. 10. SEM secondary electron images of NiAl and (Ni,Pt)Al cross-sections after 200-h oxidation at 1150°C, showing: (a) large void formed over NiAl grain boundary (arrow); (b) no voids at oxide-metal interface of (Ni,Pt)Al. However, in some locations (Ni,Pt)Al formed numerous smaller voids at the bond coat-super alloy interface. Also, note the accelerated depletion of β -phase along the NiAl coating grain boundary in (a).

In contrast to the NiAl coatings, very adherent scales were maintained on all surfaces of the (Ni,Pt)Al coatings during these tests. No scale spallation from bulk grains or grain boundaries was observed after 200-h at 1150°C, as shown by Figs. 8(c) and (d). Additionally, examination of (Ni,Pt)Al coating cross-sections by SEM after 100-h and 200-h exposure detected no visible voids at the oxide-metal interface [Fig. 10(b)]. Thus, even in the presence of relatively higher sulfur levels (as compared to the low-sulfur NiAl in this study), growth of visible oxide-metal voids was not detected in the Pt-modified coatings. However, the (Ni,Pt)Al coatings did contain significant amounts of metallic voids at the original coating-substrate interface, as shown in Fig. 10(b). It was confirmed that some of these voids were located on coating grain boundaries, but most grains in the (Ni,Pt)Al did not etch, so it was not clear what proportion of the coating-substrate voids were associated with grain boundaries.

The coating-substrate voids in (Ni,Pt)Al were generally smaller and more numerous than the voids observed at the oxide-metal interface of NiAl and exhibited a much greater distribution in size, ranging from 3–30 μm in diameter after 200 h. Small voids were observed at this interface in as-deposited (Ni,Pt)Al coatings in previous work [31], possibly due to a Kirkendall effect associated with rapid diffusion of Al from the substrate into the Pt layer during the early stages of aluminizing. The size and number of these coating-substrate voids appeared to increase in the (Ni,Pt)Al of this study with oxidation time. Comparison of Figs. 10(a) and (b) demonstrates that the voids which formed on NiAl and (Ni,Pt)Al exhibited opposite curvature. The oxide-metal voids on NiAl were concave toward the substrate, whereas the coating-substrate voids on (Ni,Pt)Al were often concave toward the coating surface. The voids grew into the aluminide coating layer in both cases.

4. DISCUSSION

4.1. Pt Effects on Refractory Element Concentrations in Aluminide Coatings

The beneficial effects of Pt additions on coating oxidation behavior have often been attributed to suppression of alloying element diffusion from the substrate into the coating. From an oxidation standpoint, these elements have the potential to accelerate the growth and degrade the adherence of a protective alumina scale [32]. Earlier studies [17] reported that a relatively thick Pt layer (~25 μm) excluded refractory metal elements from the outer PtAl_2 layer of as-deposited high-activity coatings prepared by pack cementation. However, a thinner Pt layer (~5 μm) did not exclude the refractory metals from these same coatings. Similar results were reported for two-phase ($\text{PtAl}_2 + \text{NiAl}$) coatings on various Ni-based superalloys [32].

The present study indicated little observable influence of Pt on the incorporation of refractory metals into low-sulfur, low-activity, single-phase CVD aluminide coatings. Microprobe analysis measured low concentrations of refractory elements in the single-phase (β) regions of both the CVD NiAl and (Ni,Pt)Al coating [Figs. 4 and 5]. This was most likely the result of the intrinsic high-purity of the low-activity CVD aluminizing process [11], since the coating growth mechanism primarily involves outward diffusion of Ni from the substrate to react with Al at the surface during CVD. The concentrations of Ta, W and Re were slightly higher and less uniform in the as-deposited NiAl, compared to the more homogenous distribution in (Ni,Pt)Al, but absolute comparisons must be made with caution due to the poor resolution of the microprobe technique at concentrations in the range of 1 wt%. Tantalum appeared to diffuse outward more slowly in the as-deposited (Ni,Pt)Al than in the NiAl, as there was an apparent gradient through the (Ni,Pt)Al coating region up to ~40 μm in Fig. 5(a). However, after oxidation at 1150°C, the refractory elements appeared to be uniformly distributed in the remaining β phase of both NiAl and (Ni,Pt)Al coatings [Figs. 5(b)-(c), Figs. 5(e)-(f)].

The concentrations of refractory elements (especially Ta) were much higher in the γ' region of both coatings due to the higher solubility of these elements in Ni_3Al . Therefore, if Al depletion occurs in the coating, resulting in the formation of either small γ' zones near the coating-oxide interface (due to scale spallation during thermal cycling conditions), or in regions

of γ' localized or adjacent to the coating grain boundaries (due to loss of Al by interdiffusion and scale spallation/re-growth), refractory element concentrations could allow elements such as Ta to cause local disruption of the scale through the formation of rapid-growing secondary oxides [33]. Growth of internal precipitates of these secondary oxides would almost certainly have a deleterious effect on scale adherence, especially during cyclic oxidation. Thus, if Pt has the capability to stabilize the β -phase (which has not been verified conclusively in this study), this may be more important than the tendency to serve as a diffusion barrier to refractory metal diffusion through the β -phase.

4.2. Pt Effects on Scale Growth Rates

Both NiAl and (Ni,Pt)Al coatings displayed extremely low oxidation rates, as compared to uncoated René N5'. Their oxidation rates were slightly lower than that of optimized NiAl + Hf (Fig. 1), indicating extremely slow oxide growth rates during these relatively short-term tests. Comparison of the continuous mass gain curves in Fig. 1 makes it clear that the addition of Pt did not reduce scale growth rates, since the oxidation rates of (Ni,Pt)Al at both 100 and 200-h were slightly higher than those of the NiAl coatings. These comparisons must be again viewed with some caution, since these are relatively short-term oxidation exposures and there may be differential rates of θ -alumina to α -alumina transformation for the hypo-stoichiometric CVD NiAl and the stoichiometric cast NiAl + Hf.

Previous isothermal oxidation studies of cast NiAl and NiPtAl alloys and NiAl+Hf at 1200°C [19] indicated that the addition of a reactive element, especially Hf, resulted in significant reductions in scale growth rates, alteration of scale microstructures and increased improvements in scale adherence. The reduction in scale growth rates by reactive element (RE) doping has been attributed to inhibition of outward Al diffusion along the oxide grain boundaries of RE-doped α -Al₂O₃ scales [34]. Thus, since Pt clearly improved scale adhesion in this study, but did not reduce scale growth rates, it is very likely that the Pt effect is a separate

mechanism than that induced by RE additions, as expected. However, the ~0.15wt% Hf content of the René N5' substrates must be considered a potential contributor to the extremely low oxidation rates of these coatings. The as-deposited CVD NiAl contained up to 0.14wt% Hf and the CVD (Ni, Pt)Al up to 0.08 wt% Hf near the coating/diffusion zone interface, as determined by GDMS in this study. During high temperature exposure, sufficient Hf could have diffused to the coating surface (especially along the coating grain boundaries) to alter scale growth rates, but at a concentration too low to be detected by SEM/EDS or EPMA (no GDMS of oxidized specimens has yet been performed). However, if this were the case, the level of Hf incorporation into the low-sulfur NiAl was not sufficient to significantly improve scale adherence or inhibit void formation (particularly over coating grain boundaries). It should also be noted that this level of Hf addition did not enhance scale adherence in non-desulfurized versions of the superalloy substrates. It is concluded that the extremely low growth rates of the scales on these coatings were probably due to effects other than Hf doping, such as coating grain orientation, increased Al₂O₃ scale grain size, more rapid transformation to α -Al₂O₃ due to the presence of Cr or other elements, or the large size of each single-crystal coating grain.

4.3. Pt Effects on Interdiffusion Between Coatings and Substrate Alloys

Interdiffusion can significantly influence the performance of aluminide coatings at temperatures above 1000°C, as suggested in other studies [35 - 37]. Reduction of the Al content during oxidation of aluminide coatings typically involves two processes: (1) outward loss due to oxide formation, possibly accelerated by scale spallation, and (2) interdiffusion (inward diffusion of Al and outward diffusion of Ni) with the superalloy substrate. The presence of Pt did not alter the equilibrium Al concentration in this multi-component aluminide system after homogenization. The Al content in both coatings was ~32 at% after 100 and 200-h, which does not correspond with the stability field of β -NiAl according to the binary Ni-Al phase

diagram [38]. The presence of alloying elements, such as Co and Cr probably stabilized the β phase, as suggested by Jia et al. [39]. As shown in Figs. 3 and 10(a) and Table II, depletion of β phase at 1150°C was substantial after 200-h. Since the present oxidation exposures were performed under isothermal conditions, and relatively adherent oxide scales were formed on both the NiAl and (Ni,Pt)Al coatings, there was little if any Al loss by scale spallation and re-formation. Thus, it was concluded that Al diffusion into the substrate was the major source of Al depletion in the present study.

Even though Pt incorporation did not appear to exclude refractory elements or reduce scale growth rates, there were subtle differences in the distributions of major elements in the as-deposited NiAl and (Ni,Pt)Al coatings. There was a slightly higher Al content near the coating-gas interface of the as-deposited (Ni,Pt)Al, which indicated that the diffusion behavior of Pt did not fully mirror that of Ni [40]. Aluminum was more uniformly distributed through the as-deposited NiAl coating, although there was a slight decrease in Al concentration near the coating surface. The slightly higher Al concentration near the as-deposited surface of (Ni,Pt)Al may have influenced the initial stages of oxidation and void formation behavior. However, after exposure at 1150°C for 100h and 200h, Al concentrations in the NiAl and (Ni,Pt)Al coatings were very uniform and very similar (~32 at%), as shown in Fig. 4(b).

4.4. Pt Effects on Void Formation at the Scale-Metal Interface

The surface morphologies of the oxide scales did not show significant differences as a result of the presence of Pt in the surface, since both coatings formed Al_2O_3 with the ridged or "lacy" structure [28]. However, there was a drastic difference in the growth of voids along the oxide-metal interface of NiAl and (Ni,Pt)Al. Large voids were commonly observed at the metal-oxide interface of the scale formed over the NiAl coating grain boundaries after 100-h oxidation at 1150°C [Fig. 8(a)]. Increased amounts and larger interfacial voids were found under the scale formed over the NiAl grain boundaries, as well as some grains, after 200-h

oxidation [Fig. 8(b) and Fig. 10(a)]. Interfacial voids with faceted features are commonly observed on un-doped cast NiAl, and are a primary failure mechanism for scales on cast aluminides without reactive element additions [41 - 44].

In stark contrast to the NiAl coatings, no voids were observed under the scale formed over the grains or grain boundaries on the (Ni,Pt)Al coatings after 100- and 200-h at 1150°C [Figs. 6(c), 6(d) and 8(b)]. This does not mean that very fine voids were not present in scales on (Ni,Pt)Al, but it does prove that significant interfacial void growth did not occur after 200-h, even though the Al content was reduced below the stability field of the binary NiAl system. The absence of large voids at the oxide-metal interface was the most obvious difference between the coatings, and appears to be a major reason for the improved scale adherence on the (Ni,Pt)Al coatings.

There is evidence that the tendency to form voids in hypo-stoichiometric NiAl (where Ni is the dominant diffusing species) increases as the Al content decreases [45]. It has been hypothesized that Al depletion due to oxidation at the scale-metal interface results in Ni diffusion away from the interface to the bulk to compensate for Al depletion, thus facilitating void formation [45]. It has also been postulated that Pt may reduce the apparent Al level of NiAl at which Al is the dominating diffusional element [46]. Combination of these two theories might explain the reduced tendency to form voids in (Ni,Pt)Al. However, the very low Al concentration (32 at%) in the NiPtAl coatings suggests that if Al diffusion in sub-stoichiometric β -NiAl is significantly enhanced by Pt, this effect would have to extend over a very wide concentration range. The void size distribution in NiAl suggests that voids continued to nucleate and grow in NiAl after the preliminary oxidation period (where Al concentration was approximately 39 at%). Voids did not begin to grow on NiPtAl, even after the Al content was reduced to 32 at% (prior to 100-h). This comparison suggests that the dramatic differences in void growth at the oxide-metal interface of NiAl and (Ni,Pt)Al may not be directly related to Al concentrations.

Another likely role of Pt is to mitigate the detrimental influence of sulfur impurities, as suggested by previous work [25, 26]. The presence of sulfur at the scale-metal interface is generally thought to accelerate void growth [34, 44, 47, 48, 49]. In fact, the sulfur content in the low-sulfur CVD NiAl coatings of this study (~0.5 ppmw) was still not sufficiently low to completely prevent void formation in the hypo-stoichiometric NiAl, in agreement with previous observations of low-sulfur cast NiAl [50]. In contrast, growth of interfacial voids along the coating grain boundaries was inhibited in the Pt-modified coatings in spite of the much higher sulfur levels in CVD (Ni,Pt)Al. It is also possible that the presence of solid solution Pt in the β -NiAl phase alters the segregation behavior of sulfur to either the oxide-metal interface or to the surfaces of small micro-voids that form due to perturbations at the oxide-metal interface [44]. Perhaps in the case of (Ni,Pt)Al these perturbation voids do not grow without the stabilizing influence of sulfur segregation, thus improving oxide adherence. It is also not clear whether there is critical sulfur level above which Pt may be less effective at improving scale adherence or reducing void growth. Clearly, studies of a more fundamental nature will be required in order to adequately define the mechanism(s) of the Pt effect.

Platinum may also contribute to suppressed void growth by increased bonding energy between the metallic substrate and oxide scale, thus, reducing the likelihood of small voids nucleating and growing the oxide-metal interface. It is also possible that the beneficial effect of Pt is related to a mechanical interlocking effect, since metallic protrusions from the (Ni,Pt)Al coatings into the Al_2O_3 scales were observed on the (Ni,Pt)Al but not on NiAl coatings. Similar observations were reported in earlier studies on Pt-Al alloys [16]. It is possible that these protrusions may contribute to the more adherent scale on the bulk grains. However, the interlocking mechanism does not readily account for the apparent influence of Pt to suppress void growth, particularly over aluminide grain boundaries. Thus, it is our conclusion that suppression of void growth, mitigation of sulfur effects and improve oxide-metal bond strength (which are all likely related) are more important influences on scale adherence than the observed

mechanical keying. This conclusion is also based on other observations where good alumina scale adherence is observed without mechanical keying [34].

The observed formation of voids at the substrate-coating interface (Fig. 10) may be related to preferential coalescence of vacancies on alumina particles or pre-existing Kirkendall voids along the coating-superalloy interface of (Ni,Pt)Al instead of at very fine scale perturbation voids along the oxide-metal interface of NiAl. However, why such a difference should occur is not clear.

4.5 Pt Effects on Coating Grain Boundaries

Scale adherence at coating grain boundaries may be influenced by several mechanisms, such as chemical effects (short-circuit diffusion pathways for alloying elements and sulfur impurities), geometric effects (additional stresses caused by the non-planar geometry of the grain boundary ridges), and/or preferential void nucleation and/or coalescence sites [24, 25]. Analysis of as-deposited and oxidized coating cross-sections by FEG-EDS and WDS revealed that submicron-sized particles rich in refractory elements (W, Re, Mo, and Ta) precipitated along NiAl and (Ni,Pt)Al coating grain boundaries [Figs. 6 and 7]. It is likely that these refractory-rich particles are present at the grain boundaries due to rejection of these low-solubility elements during cooling. The higher concentration of refractory elements on the coating grain boundaries may accelerate scale spallation by degrading the oxide-metal bond strength, altering the local mechanical properties (CTE, yield strength, creep behavior, etc.), by stabilizing γ' formation, or by increasing the growth rate of the oxide scale once scale spallation and re-formation begin. Although there are some discrepancies regarding the deleterious effects of refractory elements on oxidation resistance, the presence of Ta in alumina scales has been found to initiate scale failure and partially counter the beneficial effects of reactive element additions [33]. In addition, the transformation of β into γ' proceeded more rapidly along the

aluminide coating grain boundaries in this study, which was also reported for conventional two-phase Pt-modified aluminide coatings [51].

Although there was no obvious grain boundary degradation in the high-purity (Ni,Pt)Al coatings in this study, other investigators have observed preferential grain boundary degradation of commercial Pt-modified aluminide bond coatings within EB-PVD TBC systems [52]. Thus, it is clear that for these columnar-grained aluminide coating systems, the coating grain boundaries are a weak link in system performance and require significant further study.

5. SUMMARY AND CONCLUSIONS

A single-phase (Ni,Pt)Al coating was prepared by electroplating a thin layer of Pt followed by a unique low-sulfur CVD aluminizing process. Several important effects of Pt on high temperature oxidation have been observed in this study. First, Pt incorporation into the low-activity CVD single-phase aluminide coatings did not reduce scale growth rates at 1150°C. Second, Pt incorporation did not significantly exclude refractory metal elements from the substrate into the single-phase (Ni,Pt)Al coating, by EPMA analysis. Third, Pt additions did not significantly alter segregation of refractory elements to coating grain boundaries, since segregation of refractory metals to coating grain boundaries was observed for both NiAl and (Ni,Pt)Al coatings in the as-deposited and oxidized conditions. However, Pt incorporation did significantly improve scale adherence during both cyclic [25] and isothermal oxidation tests, even though the sulfur content of the (Ni,Pt)Al coatings was higher than that of the NiAl. It appears that, at the sulfur levels of this study, Pt additions to single-phase aluminide coatings can mitigate the detrimental effects of sulfur impurities on scale adherence. In concert with this, the most remarkable effect of Pt observed in the present study was the inhibition of void growth at the scale-metal interface, especially along coating grain boundaries.

ACKNOWLEDGMENTS

The authors thank C. Kortovich and L. Graham of PCC Airfoils for providing superalloy substrate material; B. Warnes and N. DuShane of Howmet Corporation for conducting Pt electroplating; L.D. Chitwood and G. Garner at ORNL for assisting with oxidation experiments; and L. Walker at ORNL for the EPMA analysis. The authors also thank Ted Besmann, Pete Tortorelli, and Mike Lance at ORNL for reviewing the manuscript. This research was sponsored by the Advanced Gas Turbine Systems Program, DOE Office of Industrial Technologies, under contract DE-AC05-96OR22464 with UT-Batelle Research Corporation.

REFERENCES

1. S.M. Meier, D.K. Gupta, and K.D. Sheffler: *JOM*, 1991, vol. 43, pp. 50-53.
2. S.M. Meier, D.M. Nissley, K.D. Sheffler, and T.A. Cruse: *Trans. ASME*, 1992, vol. 114, pp. 258-263.
3. A. Maricocchi, A. Bartz, and D.J. Wortman: *Proceedings of the 1995 Thermal Barrier Coating Workshop*, ed. W.J. Brindley, NASA Conference Publication No. 3312, 1995, pp.79-89.
4. W.P. Parks, E.E. Hoffman, W.Y. Lee, and I.G. Wright: *J. Thermal Spray Technol.*, 1997, vol. 6(2), pp. 187-192.
5. G. Lehnert and H. Meinhardt: *Electrodep. Surf. Treat.*, 1972/1973, vol. 1, pp. 189-197.
6. J.S. Smith and D.H. Boone: *ASME Paper No. 90-GT-319*, 1990, The American Society of Mechanical Engineers, New York, NY.
7. J. Schaeffer, G. Kim, G.H. Meier and F.S. Pettit: *The Role of Active Elements in the Oxidation Behavior of High Temperature Metals and Alloys*, E. Lang, ed., Elsevier Applied Science, New York, 1989, pp. 231-267.
8. M.S. Farrell, D.H. Boone, and R. Streiff: *Surf. Coat. Technol.*, 1987, vol. 32, pp. 69-84.
9. M. Göbel, A. Rahmel, M. Schütze, M. Schorr, and W.T. Wu: *Mater. High Temp.*, 1994, vol. 12, pp. 301-309.
10. W.C. Basta, D.C. Punola and B.M. Warnes: *US Patent 5,658,614*, 1997.
11. B.M. Warnes and D.C. Punola, *Surf. Coat. Technol.*, 1997, vol. 94-95, pp. 1-6.
12. B. M. Warnes and D. C. Punola: *Power Generation Technology: The International Review of Preliminary Power Production*, R. Knox, ed., Sterling Publications Limited, London, England, 1995, pp. 207-210.
13. Z. Mutasim and W. Brentnall: *ASME Paper No. 96-GT-436*, 1996, The American Society of Mechanical Engineers, New York, NY.
14. J.G. Fountain, F.A. Golightly, F.H. Stott, and G.C. Wood: *Oxid. Met.*, 1976, vol. 10, pp. 341-345.
15. E.J. Felten: *Oxid. Met.*, 1976, vol. 10, pp. 23-28.
16. E.J. Felten and F.S. Pettit: *Oxid. Met.*, 1976, vol. 10, pp. 189-223.

17. M.R. Jackson and J.R. Rairden: *Metall. Trans. A*, 1977, vol. 8A, pp. 1697-1707.
18. J.H.W. de Wit and P.A. van Manen: *Mater. Sci. Forum*, 1994, vol. 154, pp. 109-118.
19. B.A. Pint, I.G. Wright, W.Y. Lee, Y. Zhang, K. Prüßner and K.B. Alexander: *Mater. Sci. Eng. A*, 1998, vol. A245, pp. 201-211.
20. J.G. Smeggil, A.W. Funkenbusch, and N.S. Bornstein: *Metall. Trans. A*, 1986, vol. 17A, pp. 923-932.
21. J.L. Smialek: *Metall. Trans. A*, 1987, vol. 18A, pp. 164-167.
22. J.G. Smeggil and G.G. Peterson: *Oxid. Met.*, 1988, vol. 29, pp. 103-119.
23. J.C. Schaeffer, W.H. Murphy, and J.L. Smialek: *Oxid. Met.*, 1995, vol. 43, pp. 1-23.
24. W.Y. Lee, Y. Zhang, I.G. Wright, B.A. Pint, and P.K. Liaw: *Metall. Trans. A*, 1998, 29A, pp. 833-841.
25. Y. Zhang, W.Y. Lee, J.A. Haynes, I.G. Wright, B.A. Pint, K.M. Cooley and P.K. Liaw, *Metall. Trans. A*, 30A, 1999, 2679 – 2687.
26. J.A. Haynes, Y. Zhang, W.Y. Lee, B.A. Pint, I.G. Wright, and K.M. Cooley, in Elevated Temperature Coatings: Science and Technology III, The Minerals, Metals and Materials Society, 1999, Edited by J.M. Hampikian and N.B. Dahotre, pp. 185-196.
27. B.A. Pint, *Oxidation of Metals.*, 1998, 49 (5-6) pp. 531-559.
28. J. Doychak, J.L. Smialek, and C.A. Barrett: *Oxidation of High-Temperature Intermetallics*, T. Grobstein and J. Doychak eds, TMS, Warrendale, PA, 1988, pp. 41-56.
29. J. Doychak, "Oxidation Behavior of High Temperature Intermetallics," in *Intermetallic Compounds, Vol.1: Principles*, J. H. Westbrook and R. L. Fleischer eds. (John Wiley & Sons, New York, NY, 1994, p.977-1016.
30. Homma, H. M. Hindam, Y. Pyun, W. W. Smeltzer, *Oxid. Met.*, 1982, 17, 223-33.
31. R. Streiff, D.H. Boone and L.J. Purvis, "Structure of platinum modified aluminide coatings", *Surface Engineering: Surface Modification of Materials*, NATO ASI Ser, Martinus Nijhoff Publishers, Dordrecht, Netherlands, 1984, pp. 469 – 481.
32. H.M. Tawancy, N.M. Abbas, and T.N. Rhys-Jones: *Surf. Coat. Technol.*, 1991, vol. 49, pp. 1-7.

33. I. G. Wright, B. A. Pint, W. Y. Lee, K. B. Alexander, and K. Prübner, "Some effects of metallic substrate composition on degradation of thermal barrier coatings," in High-Temperature Surface Engineering, Institute of Materials, J. Nicholls and D. Rickerby, Eds., Book 693, IOM Communications Ltd. (2000) pp. 95-113.
34. B.A. Pint: *Oxid. Met.*, 1996, vol. 45, pp. 1-37.
35. J.L. Smialek and C.E. Lowell: *J. Electrochem. Soc.*, 1974, vol. 121, pp. 800-805.
36. .S. Pettit and C.S. Giggins: in "Superalloys II", edited by C.T. Sims, N.S. Stoloff and W.C. Hagel (Wiley, New York, 1987), p. 327.
37. N. Birks, G.H. Meier, and F.S. Pettit: *Superalloys, Supercomposites and Superceramics*, J.K. Tien and T. Caulfield eds., Academic Press, New York, 1989, pp. 439.
38. P. Nash, M.F. Singleton, and J.L. Murray: *Phase Diagrams of Binary Nickel Alloys*, 1991, vol. 1 (edited by P. Nash). ASM International, Metals Park, Ohio.
39. C.C. Jia, K.Ishida, and T. Nishizawa: *Metall. Trans. A*, 1994, vol. 25A, pp. 473-485.
40. R. Streiff, O. Cerclier, and D.H. Boone: *Surf. Coat. Technol.*, 1991, vol. 49, pp. 111-126.
41. J.L. Smialek: *Metall. Trans. A*, 1978, vol. 9A, pp. 309-320.
42. H. M. Hindam and W. W. Smeltzer, *J. Electrochem. Soc.*, 1980, 127, pp.1630-5.
43. A. Katsman, H.J. Grabke, and L. Levin: *Oxid. Met.*, 1996, vol. 46, pp. 313-331.
44. B.A. Pint: *Oxid. Met.*, 1997, vol. 48, pp. 303-328.
45. M.V. Brumm and H. J. Grabke, *Corrosion Science*, 1993, vol. 34, pp. 547.
46. P. Deb, H. Boone, and R. Streiff, in Proceedings of the International Conference on Surface Modifications and Coatings, Toronto, Canada, 1985, ASM, Ed., R.D. Sisson Jr., pp. 143-159.
47. H.J. Grabke, D. Weimer, and H. Viehhaus: *Appl. Surf. Sci.*, 1991, vol. 47, pp. 243-250.
48. H.J. Grabke, G. Kurbatov, H.J. Schmutzler, *Oxid. Met.*, 1995, v43, pp. 71-80.
49. P.G. Hou, and J. Stringer: *Oxid. Met.*, 1992, vol. 38, pp. 323-345.
50. C. Sarioglu, C. Stinner, J.R. Blachere, N. Birks, F.S. Pettit, G.H. Meier, J.L. Smialek, in Superalloys 1996, Edited by R.D. Kissinger, D.J. Deye, D.L. Anton, A.D. Cetel, M.V. Nathal, T.M. Pollock and D.A. Woodford, TMS, 1996, pp. 71-80.

51. Y. Niu, W.T. Wu, D.H. Boone, J.S. Smith, J.Q. Zhang, and C.L. Zhen: *J.Phys. IV*, 1993, vol. 3, pp. 511-519.
52. M. Gell, K. Vaidyanathan, B. Barber, J. Cheng and E. Jordan, *Met. Trans. A*, 30A, 1999, pp. 427-435.